

Aqueous impregnation of porous β -tricalcium phosphate scaffolds

C. Stähli^a, M. Bohner^{a,*}, M. Bashoor-Zadeh^b, N. Doebelin^a, G. Baroud^b

^aRMS Foundation, Bismattstrasse 12, CH-2544 Bettlach, Switzerland

^bLaboratoire de Biomécanique, Département de Génie Mécanique, Université de Sherbrooke, Sherbrooke, QC, Canada J1K 2R1

ARTICLE INFO

Article history:

Received 11 November 2009

Received in revised form 21 December 2009

Accepted 11 January 2010

Available online 18 January 2010

Keywords:

Tissue engineering

Calcium phosphate

Scaffold

Pore

Bone substitute

ABSTRACT

The ability of a porous bone graft substitute to be impregnated with an aqueous solution is of great importance for tissue engineering and in vivo applications. This study presents an impregnation test setup and assesses the effect of various synthesis parameters such as sintering temperature, composition, macroporosity and macropore size on the impregnation properties of porous β -tricalcium phosphate scaffolds dipped in water. Among those parameters, the macropore size had by far the largest effect; generally, the bigger the macropore size, the lower the saturation level. The results also showed that impregnation was less complete when the samples were fully dipped in water than when they were only partially dipped, owing to the requirement for the system to create air bubbles under water.

© 2010 Acta Materialia Inc. Published by Elsevier Ltd. All rights reserved.

1. Introduction

Calcium phosphate scaffolds have proved to be excellent bone substitute material since their introduction in the late 1960s [1–3]. Typical applications include knee osteotomy [4,5] or periodontal defects [6]. These scaffolds are generally very porous and bioresorbable to allow a rapid turnover from a defect filled with a ceramic to a mature and mechanically stable bone. This process is favored by the presence of pore interconnection sizes >0.05 mm, because blood vessels and cells can rapidly invade the scaffold, hence favoring ceramic bioresorption and bone ingrowth [7–9]. Despite their widespread use, few studies have addressed the handling properties of bone scaffolds, such as the ease of impregnating them with an aqueous solution (e.g., platelet-rich plasma, antibiotic solution, marrow extract, blood or a cell-culture medium). Even though the handling properties are scientifically not as relevant as the chemical, physical or biological properties, they are of paramount importance for the users (clinicians) and may dictate the commercial success or failure. For example, slightly hydrophobic behavior of a bone scaffold might lead to complaints because surgeons generally soak bone scaffolds in an aqueous liquid before use. Similarly, tissue engineers expect perfect impregnation of porous scaffold with the cell-culture medium because incomplete scaffold impregnation might impair cell growth and proliferation.

Recently, attention has been drawn to the observation that two distinct β -tricalcium phosphate (β -TCP) scaffolds with similar porosity (70–75%) and macroporosity (mean pores >0.05 mm in diameter; 50–55%) could behave in different ways in impregnation tests. Therefore, it was decided to study the effect of various factors (sintering temperature, Ca/P molar ratio, presence of macropores, macropore size) on the ability of β -TCP scaffolds to be impregnated with an aqueous solution. Water was used for that purpose for three reasons: (i) water is much easier to obtain and handle than (clotting) blood; (ii) scaffolds can be tested several times provided they are dried after testing; and (iii) several handling tests made with blood did not reveal significant changes compared with tests made in water.

2. Materials and methods

Blocks were produced by the so-called “calcium phosphate emulsions” method [10,11], which is used to produce commercially available bone substitute (chronOS™, Synthes Biomaterials, USA). The main starting material was α -tricalcium phosphate (α -TCP). The powder was produced by mixing dicalcium phosphate (GFS No. 1548; USA) and calcium carbonate (Merck No. 1.02066, Dietikon, Switzerland; 2.22:1 molar mixture to get a Ca/P molar ratio of 1.45). The powder was then calcined at 900 °C for 1 h, briefly ground with a pestle and mortar until it could pass through a 0.5-mm sieve, sintered at 1400 °C for 4 h and then rapidly cooled. Further, the resulting cake was ground in a jaw crusher (BB51 Jaw Crusher, Retsch, Germany; interpolate distance 1 mm) and milled for 6 h in a 1.9-L polyethylene jar rotating at 50 rounds per minute

* Corresponding author. Tel.: +41 326441413; fax: +41 326441176.

E-mail addresses: actabio.bohner@bluewin.ch, marc.bohner@rms-foundation.ch (M. Bohner).

(370 g powder, 280 g ethanol, 3.6 kg ZrO_2 1.3 × 1.3 cm cylindrically shaped grinding media). Finally, the powder was dried, sieved (with a 0.125-mm sieve to remove some residual large particles) and calcined at 500 °C for 1 h. According to X-ray diffraction (XRD), the starting α -TCP powder contained 97% α -TCP, 2% β -CPP and no detectable amount of β -TCP and HA.

The macroporous β -TCP blocks were produced by a method developed in house [10]. This method, which is based on the use of calcium phosphate cements, allows good and easy control of macropore size. To produce one batch of blocks, 80 g of a mixture of α -TCP and calcium carbonate ($CaCO_3$; Merck No. 1.02066, Dietikon, Switzerland; see hereafter for exact mixture composition) and 20 g tricalcium phosphate powder (Merck No. 1.02143, Dietikon, Switzerland) were added to 100 g viscous paraffin oil (Merck No. 107160, Dietikon, Switzerland) and 67 mL of a solution containing polyethoxylated castor oil (PECO; product name “Cremophor EL”, BASF No. 15-2015, Wädenswil, Switzerland), 1% 5.1 kDa poly(-acrylic acid) (Fluka No. 81132, Buchs, Switzerland), and 0.2 M Na_2HPO_4 solution. These components were stirred at 2000 rpm with a four-wing impeller for 45 s (Eurostar Digital, IKA, Germany). The resulting paste consisted in a metastable mixture of a calcium phosphate cement paste in which small oil droplets were dispersed. After 150 s, the resulting paste was poured into eight moulds, incubated for 24 h until complete hardening occurred, cleaned with petroleum ether (Merck No. 1.00915, Dietikon, Switzerland), and dried. The samples produced without oil had the same composition as those with oil except for the absence of oil. Three batches of macroporous samples (with oil) and six batches of microporous samples (without oil) were produced for each Ca/P molar ratio. The Ca/P molar ratio was controlled by the amount of calcium carbonate in the starting powder mixture: 0, 1.27, 2.50 g $CaCO_3$ for 80, 78.73 or 77.50 g α -TCP, leading to a Ca/P molar ratio of 1.45, 1.475 and 1.500. The 3 × 8 samples produced for each Ca/P molar ratio were then distributed into six groups, and each group was sintered at a different temperature: 1000, 1100, 1150, 1200, 1250 and 1350 °C. Afterwards, the samples were machined to obtain cylinders 14 mm in diameter and 14 mm long. Typically, one to three cylinders were obtained per sample, depending on the sample size. For non-macroporous samples (produced without oil), lathing was so difficult that most samples broke, and very few intact cylinders could be obtained.

In addition to samples produced with different Ca/P molar ratios and sintered at different temperatures, other samples were produced according to the same method used for the samples described herein, but with various emulsifier concentrations, hence leading to samples with macropore diameters in the range 0.15–1.2 mm [11]. These samples had a Ca/P molar ratio of 1.50 and were sintered at 1250 °C. Later, the samples were lathed to diameter 8 mm and length 13 mm. The detailed production, characterization and in vivo performance of these samples have been published elsewhere [9,11–13].

The cylindrical blocks were characterized by several means: (i) scanning electron microscopy (SEM) to analyze their microstructure; (ii) XRD to assess their crystalline composition; (iii) impregnation tests to investigate their impregnation rate and extent; (iv) compressive tests to determine their compressive strength; and (v) micro-computed tomography (mCT). The following paragraphs briefly review how these characterizations were performed.

For SEM, broken pieces of the blocks retrieved after compressive testing were coated with gold and observed with an EVO MA25 microscope (Zeiss, Germany). Special attention was paid to the microstructure of ruptured surfaces. For XRD, block remnants were homogenized and packed in a cavity in an aluminum sample holder. XRD data were collected in reflective geometry on a Philips PW1800 diffractometer (Philips, Eindhoven, the Netherlands)

equipped with a graphite monochromator in the secondary beam. $Cu K\alpha$ radiation and a step size of 0.02° were used to measure from 4.01 to 59.99° 2θ . Rietveld refinements for quantitative phase analysis were done with the FullProf.2k computer program (Version 3.40) [14] using a previously determined instrument resolution function. Starting models for the quantified phases were taken from Dickens et al. [15] for β -TCP (whitlockite model, but with fully Ca-occupied sites), Mathew et al. [16] for α -TCP, Sudarsanan and Young [17] for hydroxyapatite, and Boudin et al. [18] for β -calcium pyrophosphate.

To test impregnation, a test setup used to determine the cohesion of ceramic paste [19] was slightly modified (Fig. 1). The impregnation setup consisted of a beaker filled with 500 ml of distilled water and a cylinder holder which was placed on a scale and allowed to adjust the vertical position of the cylinder. The scale (PR5002, Mettler Toledo, Switzerland) was connected to a computer (Mettler Toledo LC-R59 Cable) and the data (date/time and weight) were retrieved with special software (Mettler Toledo Balance Link, Version 4.0.0). Each sample was first weighed before dipping it, in order to measure its dry weight W_{dry} . Then, the scale was tared and the sample dipped according to the two different methods, called “partial dip” or “full dip” (Fig. 1). Both methods applied the same principle: the cylinder was fixed into a thin metallic brace held by a frame placed on a scale, the cylinder was then lowered into water, and the change in weight was recorded over time until no more changes occurred. More specifically, in the partial-dip method, the cylinder tip was dipped 2 mm into water, whereas in the full-dip method, the block was fully dipped and was covered by 5 mm of water. The cylinder weight was measured until the absorption was finished, with the last value stored as ΔW . Finally, the block was raised out of the water without touching the drop forming underneath, and its weight was measured again and stored as W_{abs} . After each test, the cylinder was treated thermally at 500 °C for 60 min. Since it was difficult to identify the cylinder orientation, samples were randomly positioned in the metallic brace.

The time required to impregnate the samples (“impregnation time”) and the porous fraction filled with water (“saturation”) were determined from these tests. The details of the calculations made to determine the impregnation time and the saturation are given in the Appendix. It is important to mention that too rapid weight changes could not be monitored with the scale because the scale gave delivery values only when the weight was “relatively” constant. This was an important drawback for the determination of the impregnation rate, but unfortunately could not be solved.

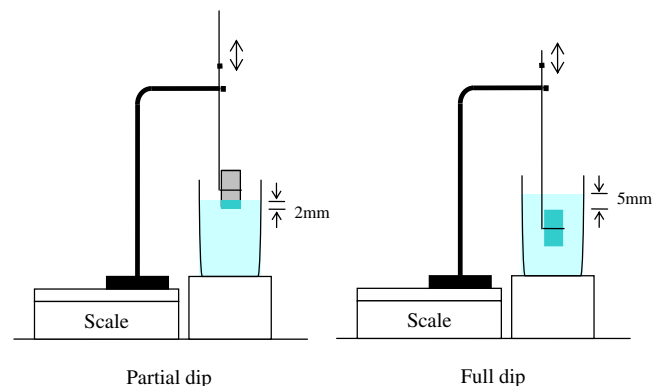


Fig. 1. Schematic representation of the setup used to measure the impregnation rate. Two types of procedure were followed: (i) partial dip, during which only the bottom 2 mm of the samples were dipped in water; (ii) full dip, during which the sample was fully dipped in water, 5 mm under the water surface.

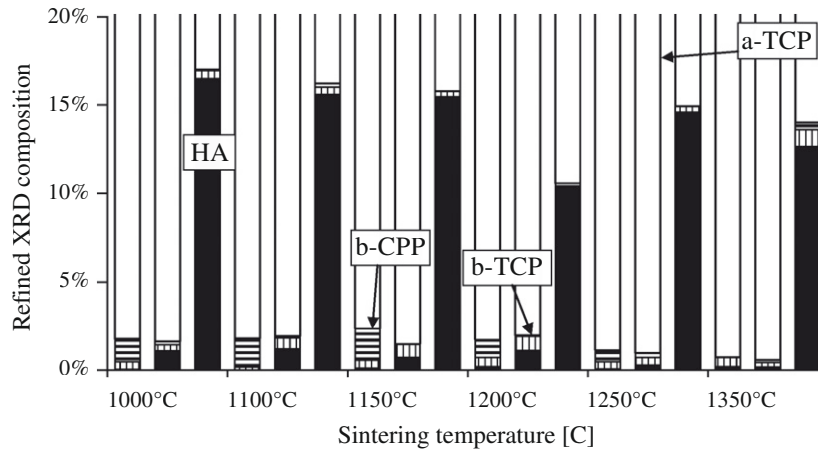


Fig. 2. Refined XRD data showing the effect of composition and sintering temperature on the crystalline block composition: black histogram bars, HA; white bars, α -TCP; bars with vertical lines, β -TCP; bars with horizontal lines, β -CPP.

The compressive strength was determined at a loading rate of 0.5 mm min^{-1} using a Zwick 1474 testing machine (Zwick, Germany). Up to six samples were tested per composition and sintering temperature.

The cylindrical samples were scanned using a SKYSCAN 1172 micro-CT scanner (Skyscan, Desktop X-ray Microtomograph, Aartselaar, Belgium) at an isotropic resolution of $15 \mu\text{m}$. Owing to the samples' properties, the X-ray tube voltage was changed in the range 55–80 kV to optimize the contrast of the recorded radiographic images. To reduce the beam hardening artefacts, a copper

plus aluminum filter was used to cut the low-energy X-ray radiations. A rotation step of 0.4° was set within an angular range of 360° , and therefore a total of 900 radiographic images with 2000×1048 pixels were acquired for each sample. NRecon software (Skyscan, Version 1.5.1.5, Aartselaar, Belgium) was then applied to reconstruct a three-dimensional structure from two-dimensional radiographic images and generate two-dimensional cross-sectional images. Finally, images of the cubic core volume with side length 7.5 mm (500 voxel) were selected as the volume of interest, and the geometric parameters were characterized.

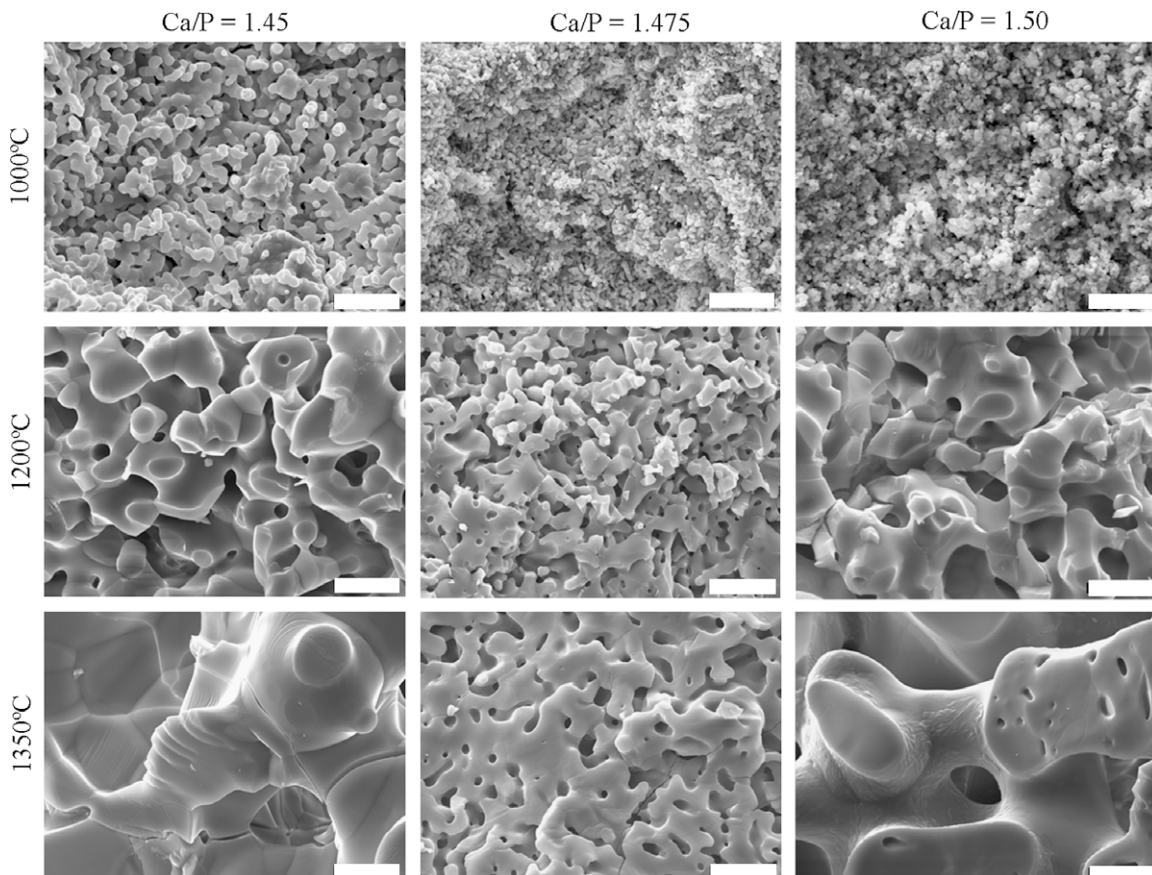


Fig. 3. SEM photos of microporous blocks for sintering temperatures 1000, 1200 and 1350 °C and different Ca/P ratios. Scale bars $10 \mu\text{m}$.

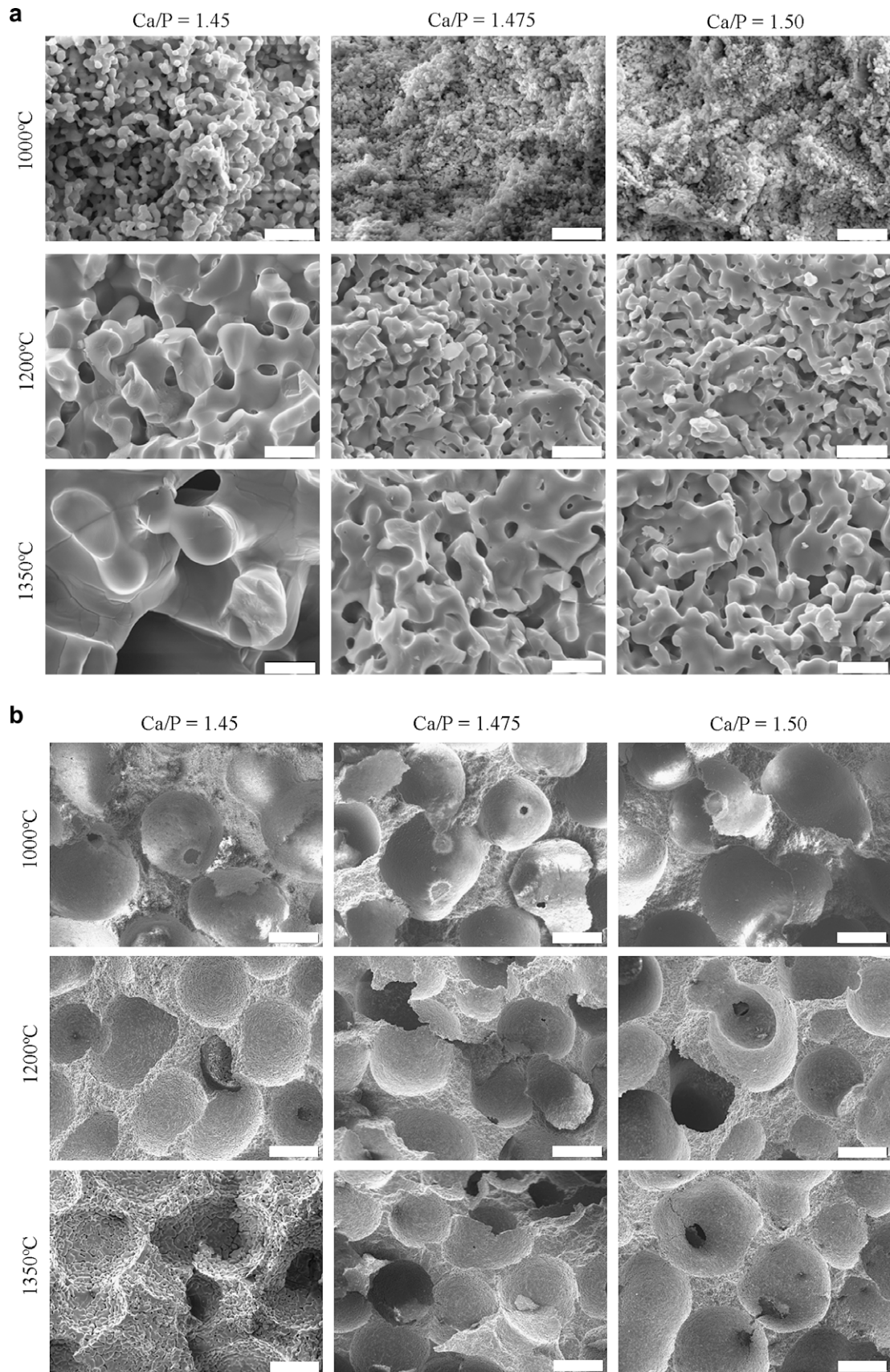


Fig. 4. SEM photos of the block microstructure for sintering temperatures 1000, 1200 and 1350 °C and different Ca/P ratios, showing: (a) microporosity (scale bar 10 μm); (b) macroporosity (scale bar 200 μm).

Considering the extent of mCT data processing, only nine samples were analyzed. These macroporous samples had three Ca/P molar ratios (1.45, 1.475 and 1.50) and were sintered at three temperatures (1000, 1200 and 1350 °C). Porosity, pore size and pore interconnection size were determined according to a recently published method [12].

3. Results

The phase composition of the emulsified blocks as determined by Rietveld refinement of XRD spectra is presented in Fig. 2. The emulsified scaffolds contained some β -calcium pyrophosphate (β -Ca₂P₂O₇; β -CPP) at a Ca/P molar ratio of 1.45 (1.1%; standard deviation (SD) = 0.7%), some hydroxyapatite (Ca₁₀(PO₄)₆(OH)₂; HA) at a Ca/P molar ratio of 1.475 (0.8%; SD = 0.5%), and a larger HA fraction at a Ca/P molar ratio of 1.50 (14%; SD = 2%). Rietveld refinement revealed the presence of <1% α -TCP in most samples, but no α -TCP peaks were visible on the XRD spectra. Importantly, the detection limit was close to 1%, which means that small changes in phase content (<1–2%) were not significant enough to draw conclusions.

The effect of sintering on the pore morphology of the blocks is clearly visible in Fig. 3 (microporous blocks) and Fig. 4 (macroporous blocks). Generally, an increase in sintering temperature provoked an increase in the micropore size (Figs. 3a and 4a). This effect was much stronger for a Ca/P molar ratio of 1.45 and 1.50 in microporous samples and for a Ca/P molar ratio of 1.45 in macroporous samples. Comparison of Fig. 3 with Fig. 4 shows that the presence of macropores only affected the block micropores for a Ca/P ratio of 1.50 (the microstructure of several samples were looked at to verify this surprising result). As expected, the macropore dimensions (Fig. 4b) were not markedly modified by a change in Ca/P ratio or sintering temperature.

The sintering temperature had a strong effect on the block porosity (Fig. 5). Specifically, the porosity of microporous blocks was reduced from 57–62% at 1000 °C to 32–35% at 1150 °C. For macroporous blocks, the reduction was from 77–83% at 1000 °C to 66–72% at 1150 °C. Interestingly, the porosity of all blocks was slightly increased with an increase in sintering temperature from 1150 to 1350 °C. Moreover, the Ca/P molar ratio affected porosity: the lower porosities were measured with a ratio of 1.475, followed by ratios of 1.50 and 1.45 ($p < 0.01$).

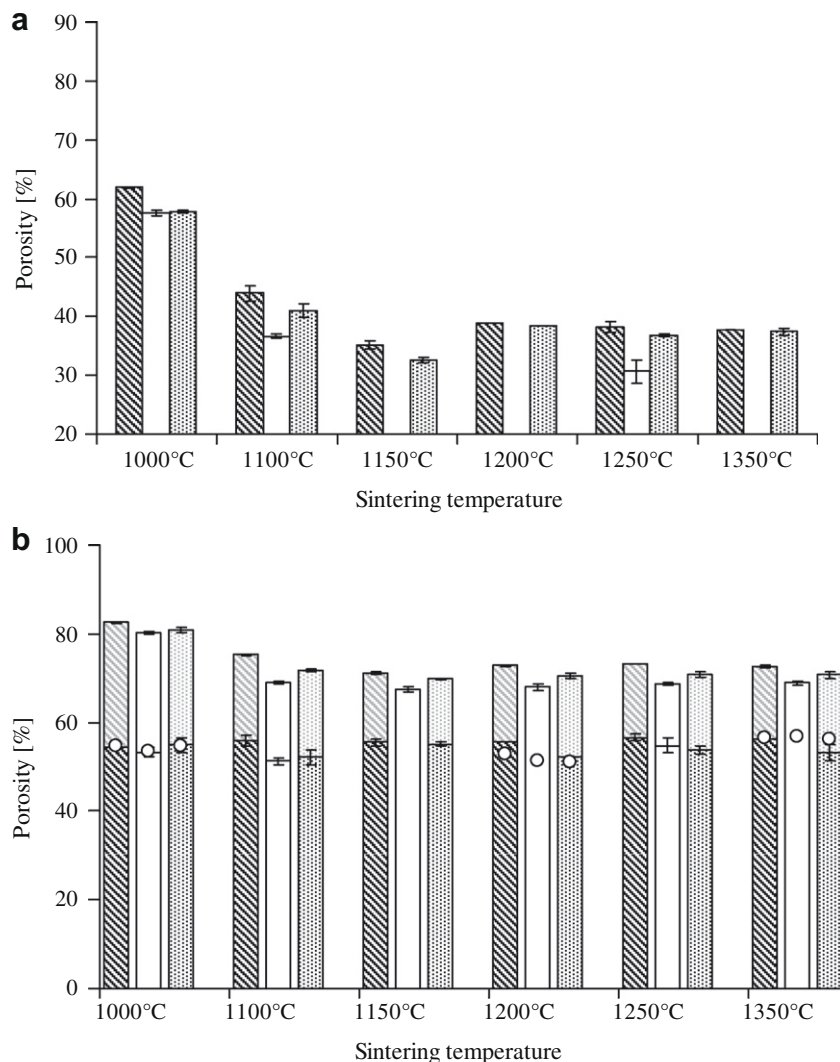


Fig. 5. Evolution of the porosity of (a) microporous and (b) macroporous cylinders as a function of sintering temperature and Ca/P ratio (using Eq. (1)). In (b), the total porosity of macroporous blocks is presented as the sum of the macroporosity (lower part of the bars) and the microporosity (upper part) calculated according to Eqs. (13) and (14). The white circles indicate the macroporosity values determined by mCT. The error bars correspond to \pm SD (hatched bars, Ca/P = 1.45; white, Ca/P = 1.475; gray, Ca/P = 1.50).

Table 1

Geometric features of the three macroporous compositions sintered at three temperatures (1000, 1200 and 1350 °C). The standard deviation is indicated within parentheses. The only results that were not deducted from mCT data analysis are the “calculated” macroporosity values, calculated using Eq. (13). Since no samples could be lathed with a Ca/P molar ratio of 1.475 and a sintering temperature of 1200 and 1350 °C, no “calculated macroporosity” was indicated for these synthesis conditions. Importantly, only one sample was measured per synthesis condition, but past studies on samples produced in these conditions showed that reproducibility was high [12]. The macroporosity could also be calculated based on the emulsion composition, assuming that it corresponds to the volume fraction of paraffin. The value was 53.6% [11], in good agreement with the other values.

Ca/P molar ratio (nominal value)	Sintering temperature (°C)	Macroporosity (%)	Macroporosity (calculated) (%)	Pore size (number) (µm)	Pore size (volume) (µm)	Interconnection size (number) (µm)
1.45	1000	54.7 (1.0)	54.4 (0.6)	272 (105)	373 (91)	44 (41)
1.475	1000	53.5 (0.9)	53.2 (2.0)	252 (92)	334 (76)	41 (35)
1.50	1000	54.6 (1.0)	54.9 (2.4)	259 (95)	345 (80)	46 (38)
1.45	1200	52.8 (0.8)	55.5 (–)	232 (86)	309 (72)	39 (31)
1.475	1200	51.3 (0.7)	–	210 (74)	274 (62)	37 (27)
1.50	1200	51.1 (0.8)	52.3 (–)	207 (72)	268 (59)	36 (27)
1.45	1350	56.6 (0.9)	56.2 (–)	233 (86)	313 (74)	41 (33)
1.475	1350	56.9 (1.0)	–	212 (80)	287 (70)	46 (34)
1.50	1350	56.3 (0.8)	53.1 (2.8)	216 (75)	283 (69)	42 (32)

The mCT results revealed no statistically significant changes in macropore size and macropore interconnection size between the nine samples investigated (Table 1; note that the mCT resolution used in this study (15 µm) enables the detection of only macropores). The volume-based macropore diameter and the interconnec-

tion size varied in the range 268–373 µm and 36–46 µm, respectively. Good agreement was found between the porosity determined by mCT (between 51.1% and 56.9%), the macroporosity determined by Eq. (13) (between 52.3 and 56.2%), and the macroporosity determined from the oil volume fraction (53.6%).

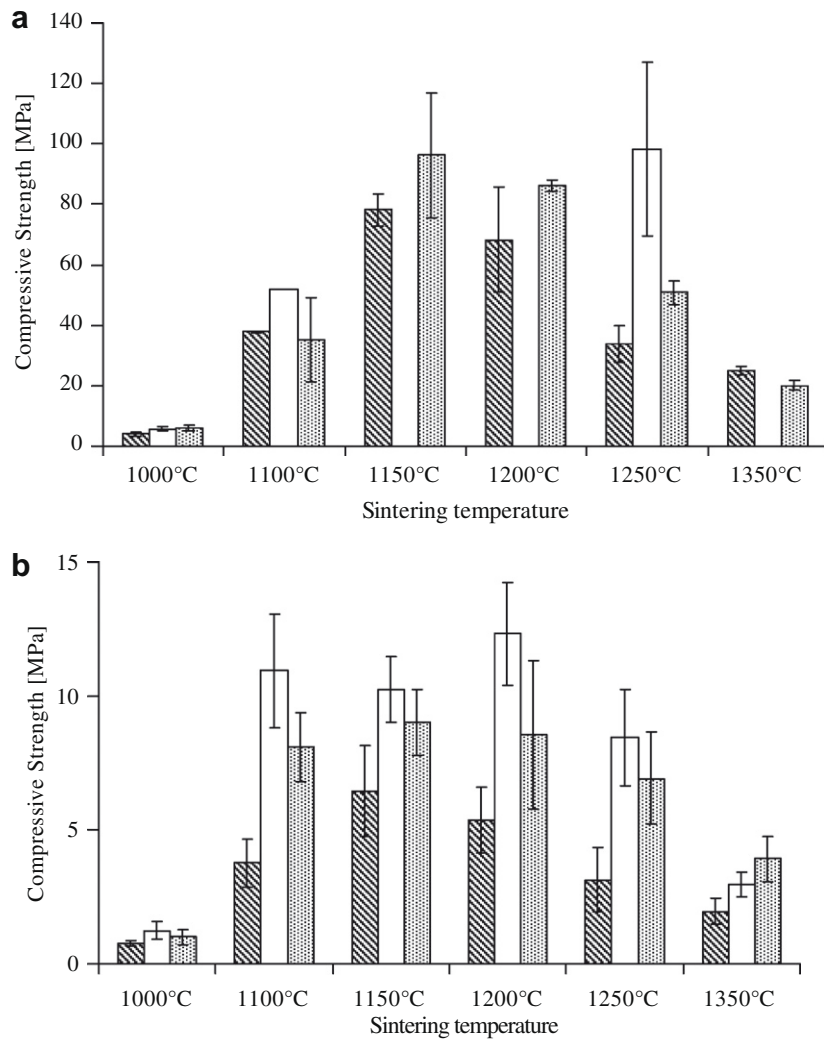


Fig. 6. Compressive strength as a function of sintering temperature and Ca/P ratio for (a) microporous and (b) macroporous blocks. For each temperature, three results are presented, corresponding to a composition of (from left to right): Ca/P = 1.45 (hatched bars); Ca/P = 1.475 (white bars); Ca/P = 1.50 (gray/dotted bars). The error bars show the SD over the six tested samples (only 1–4 in the case of microporous blocks).

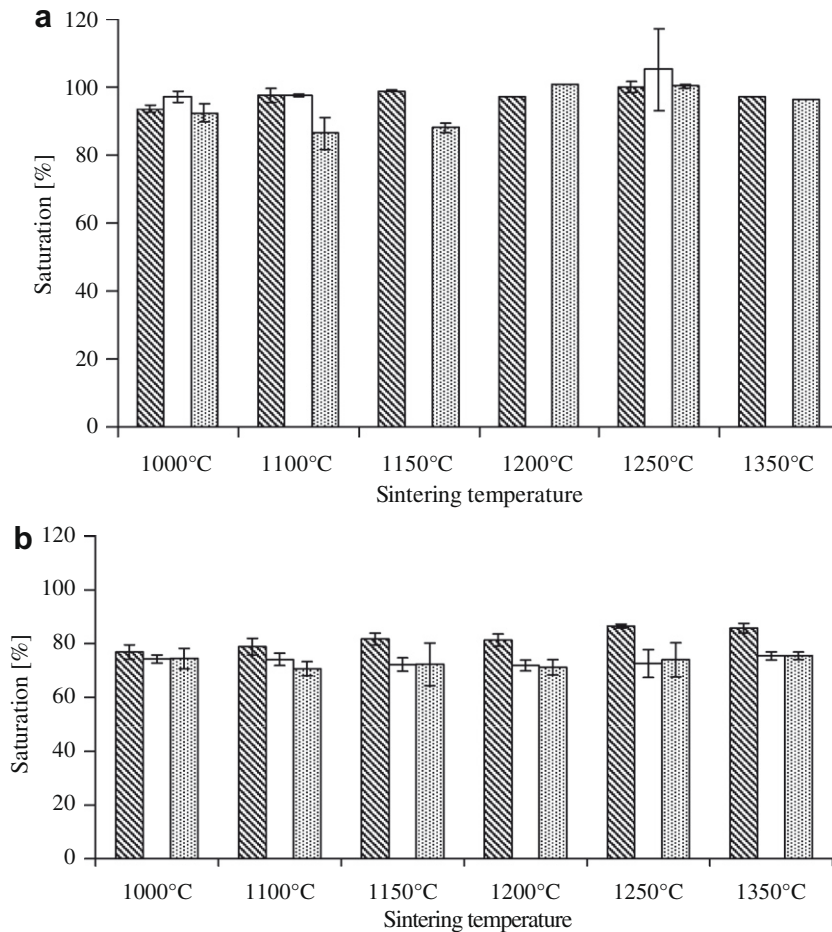


Fig. 7. Partial-dip impregnation results (saturation) as a function of sintering temperature and Ca/P ratio for (a) microporous and (b) macroporous cylinders. For each temperature, three results are presented, corresponding to a composition of (from left to right): Ca/P = 1.45 (hatched bars); Ca/P = 1.475 (white bars); Ca/P = 1.50 (gray/dotted bars).

Sintering temperature and Ca/P ratio also affected the mechanical properties of the scaffolds. Fig. 6 shows the compressive strength of (a) microporous and (b) macroporous blocks. The compressive strength of microporous samples was about one order of magnitude higher than that of the corresponding macroporous samples. However, the distribution of compressive strength with sintering temperature of the two types of samples was very similar, showing low values at 1000 °C, a maximum around 1150 and 1200 °C and a decrease towards 1350 °C. In the case of macroporous samples, the compressive strength was <2 MPa for blocks sintered at 1000 °C but increased to >10 MPa at medium sintering temperatures (for a Ca/P ratio of 1.475) before decreasing to 2–5 MPa at 1350 °C. Moreover, the influence of the chemical composition became apparent, with blocks at a Ca/P ratio of 1.45 presenting the lowest compressive strength, followed by Ca/P = 1.5 and 1.475 (significance between 1.45 and the two higher Ca/P ratios: $p < 0.05$ at 1000 °C and $p < 0.01$ at all other sintering temperatures). Samples with various macropore sizes had compressive strengths in the range 2.2–3.7 MPa, without any significant effect of pore size [9].

Generally, the sintering temperature and the Ca/P molar ratio had only a small influence on the amount of water absorbed by partially dipped samples (Fig. 7). For example, microporous samples had 90–100% of their porosity filled with water. Similarly, macroporous samples prepared with a Ca/P molar ratio of 1.475 and 1.50 presented saturation values between 71% and 75% at all sintering temperatures. A small but significant effect of Ca/P molar

ratio was observed between samples prepared with a Ca/P molar ratio of 1.45 and samples prepared with the two larger Ca/P molar ratios ($p < 0.01$ at all sintering temperatures except 1000 °C); the saturation of samples with a Ca/P molar ratio of 1.45 increased from 75–78% at 1000 °C to 84–87% at 1250 and 1350 °C ($p < 0.01$).

The results of impregnation tests carried out using the full-dip method are presented in Fig. 8. The trends seen for this method were the same as those seen in the partial-dip method. However, the saturations were generally lower in the full-dip method compared with the partial-dip method: about 10% for microporous samples and 20–30% for macroporous samples. Furthermore, an increase in the sintering temperature of macroporous samples from 1200 to 1350 °C led to a marked increase in saturation for all samples ($p < 0.01$ for all samples).

The times necessary to impregnate the blocks are presented in Fig. 9 and Fig. 10 for the partial-dip and full-dip methods, respectively. Generally, little difference in impregnation time was observed between different sintering temperatures and between microporous and macroporous samples. Most impregnation times were relatively short, in the range 10–50 s. Another general observation is that the impregnation times were shorter in the full-dip method compared with the partial-dip method.

The macropore diameter had a very large effect on the saturation results (Fig. 11a). In the partial-dip mode, the values decreased monotonically from 100% to 70% when the macropore diameter decreased from 0.15 to 1.2 mm. In the full-dip mode, the values

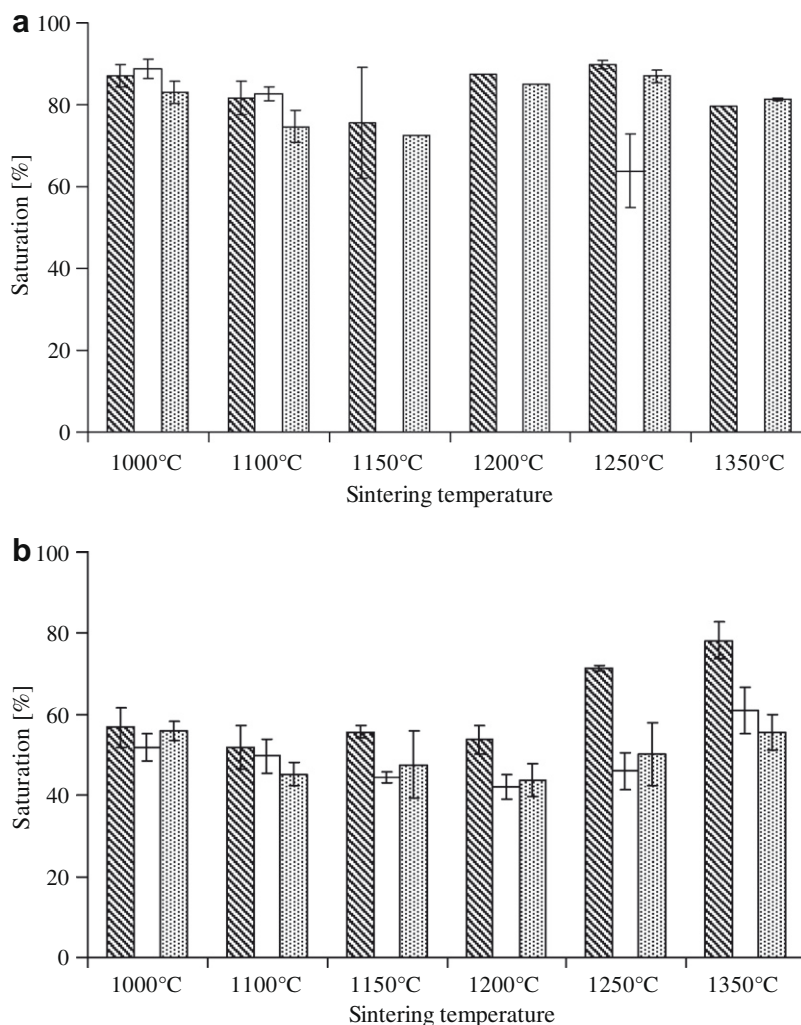


Fig. 8. Full-dip impregnation results (saturation) as a function of sintering temperature and Ca/P ratio for (a) microporous and (b) macroporous cylinders. For each temperature, three results are presented, corresponding to a composition of (from left to right): Ca/P = 1.45 (hatched bars); Ca/P = 1.475 (white bars); Ca/P = 1.50 (gray/dotted bars).

ranged between 90% and 55%. The impregnation time was also affected by the macropore diameter and the dipping method (Fig. 11b). A slight but significant increase in the impregnation time was noticed when the macropore diameter increased from 0.15 to 1.2 mm. Also, the impregnation time was shorter in the full-dip method compared with the partial-dip method.

4. Discussion

The aim of this study was to determine factors affecting the ability of a porous β -TCP scaffold to be impregnated with an aqueous solution. For that purpose, scaffolds were produced using various compositions, sintering temperatures and fractions of porogenic agent. These scaffolds were then impregnated with water using two dipping modes, one for which only a small part of the porous scaffold was dipped and one for which the porous scaffold was fully dipped. The results revealed that most tested parameters affected the saturation, but at various levels. The aim of the present discussion is to analyze and interpret the results, first by looking at the relation between synthesis conditions and properties, then by making some theoretical considerations, and finally by relating the scaffold structure and composition to the impregnation results.

Sintering β -TCP scaffolds follows complex rules, as evidenced by past studies on the topic [20–24]. The results presented in this study are generally in good agreement with past observations. For example, the drastic increase in grain size observed with a decrease in Ca/P molar ratio (Figs. 3 and 4) was mentioned by Descamps et al. [20] and Miranda et al. [23]. Similarly, the local minimum of porosity seen close to a sintering temperature of 1150 °C (Fig. 5) confirms the results of Ryu et al. [24]. Complex results were obtained for the compressive strength, since an increase to 1150–1200 °C was observed, followed by a drop at higher temperatures (Fig. 6). Earlier, Akao et al. [25] noticed a continuous increase in compressive strength with an increase in sintering temperature. However, various authors have reported the need to choose a sintering temperature for β -TCP scaffolds below the β -TCP- α -TCP transition temperature (\sim 1150 °C) to prevent this transformation and the concomitant decrease in compressive strength [24,26]. In the present study, negligible amounts of α -TCP were detected by XRD ($<$ 1%; Fig. 2), but larger amounts of α -TCP may have formed during sintering and disappeared during cooling. Since slight variations in composition have a large effect on the β -TCP- α -TCP phase transition temperature (1120 °C) [27], the low compressive strengths of the samples produced with various macropore sizes could be due to a slightly

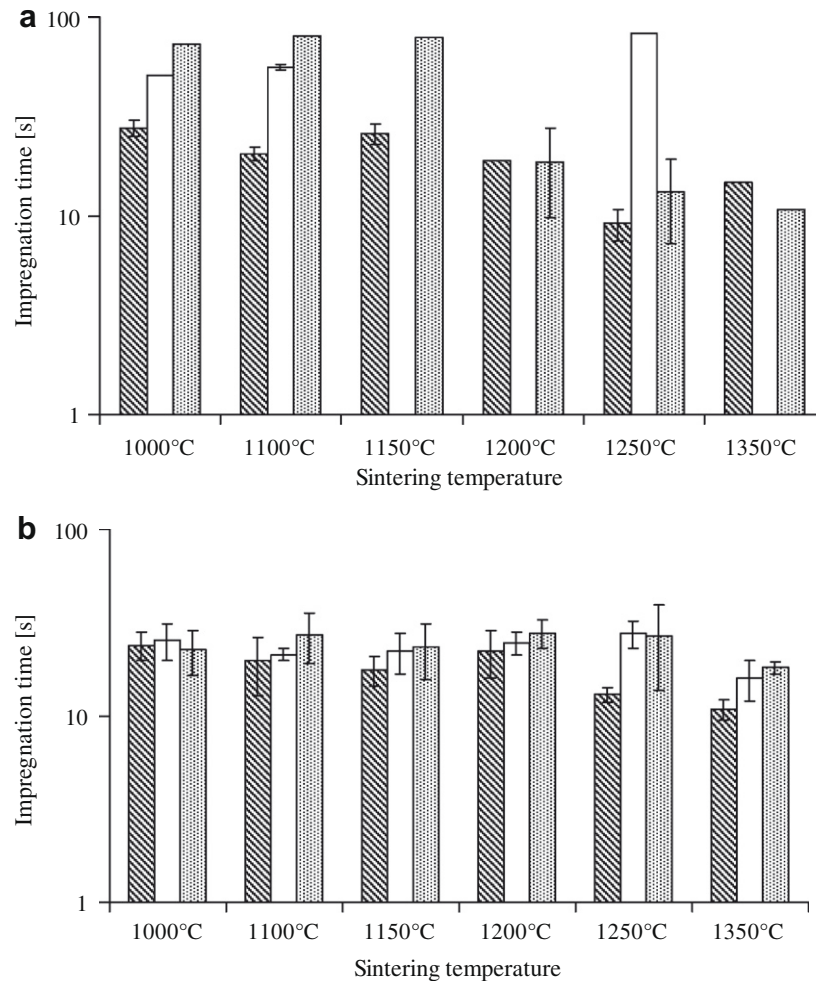


Fig. 9. Time to impregnate (= impregnation time) (a) microporous and (b) macroporous samples as a function of sintering temperature and Ca/P ratio according to the partial-dip method. For each temperature, three results are presented, corresponding to a composition of (from left to right): Ca/P = 1.45 (hatched bars); Ca/P = 1.475 (white bars); Ca/P = 1.50 (gray/dotted bars).

different composition compared with the samples produced at various sintering temperatures.

The impregnation results proved to be highly reproducible, even though the position of the sample in the metallic brace (“head” up or “head” down) was not checked. This result suggests that the sample microstructure was very homogeneous and not dependent on the sample face in contact with the liquid. Importantly, reproducibility was low when the samples were dried at a much lower temperature (105 °C) than 500 °C: the cylinders became more hydrophobic, and cylinder impregnation time became increasingly long. This effect is believed to be due to the presence of paraffin remnants in the drying cupboard, since the cupboard was also used to incubate the calcium phosphate emulsions (containing paraffin) used to produce the β -TCP scaffolds.

One indirect and one direct approach can be used to determine the amount of water trapped in partially dipped samples. In the indirect approach, the weight of the sample is measured at the end of the impregnation test and corrected to account for Archimedes force. This approach has the advantage that the sample is in static conditions (no weight change), but the correction factor depends on the dipping depth, which is difficult to set perfectly. In the direct approach, the sample is pulled out of the water at the end of the impregnation test, and the weight is measured. This method does not require any correction factor, but the drop that is present underneath the sample when the sample is pulled out of the liquid may not only be the water streaming back out of

the block porosity, but possibly also some water pulled out of the beaker as a result of surface tension and capillary forces at the cylinder surface. Thus, the saturation derived from the direct approach might slightly overestimate the real saturation. Nevertheless, the direct method for the partial-dip method was used in the present study.

Several simple theoretical considerations can be used to understand what happens when a porous scaffold is dipped into water and impregnation occurs. Two conditions must be fulfilled: (i) water must be able to penetrate the porous network through capillary rise; and (ii) air must leave the scaffold to leave space for the liquid (in the present case, water). The capillary pressure p_c provoking the penetration of the liquid into the porous network is expressed by the Young–Laplace equation:

$$p_c = \frac{2\gamma \cos \theta}{r_c} \quad (1)$$

In this equation, r_c is the capillary radius, γ is the surface tension between air and water, and θ is the wetting angle (between liquid and solid) [28]. Therefore, pores of different sizes present different capillary pressures: the smaller the pores, the larger the capillary pressure. Capillary rise will proceed as long as air can move out of the capillary under the capillary pressure. Several causes might hinder air from leaving the capillary, as represented schematically in Fig. 12: (i) the capillary is closed on one side, so the capillary rise stops when the pressure of the trapped air has reached the capil-

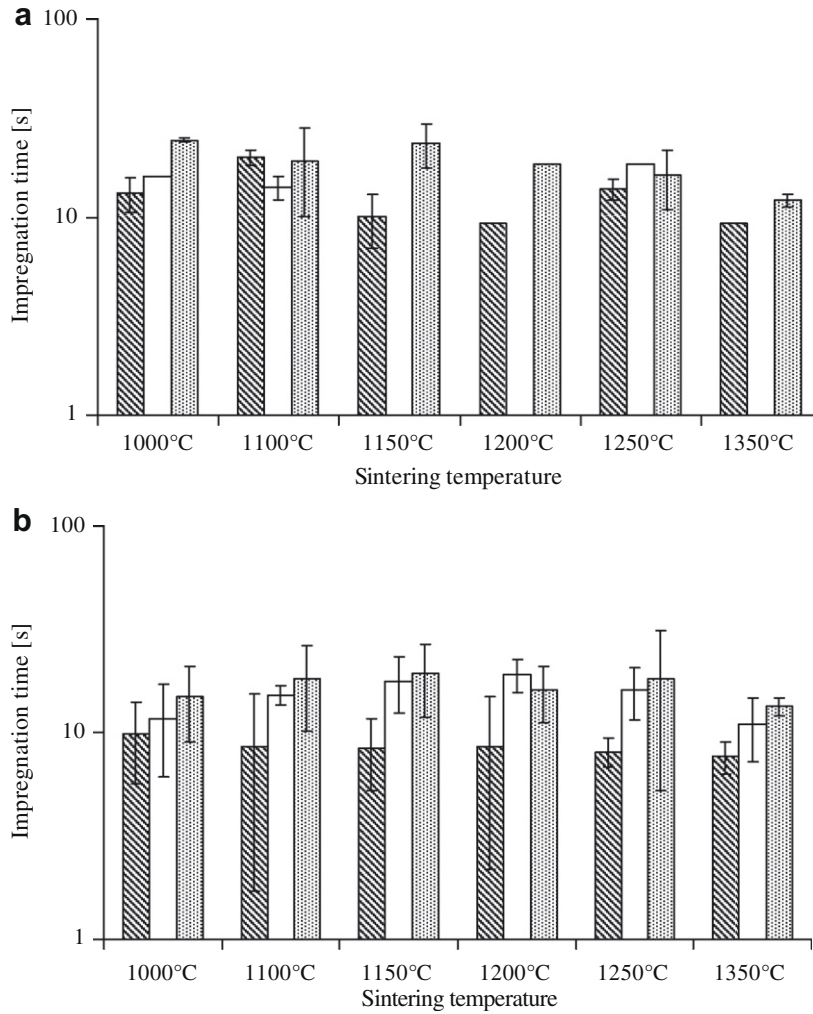


Fig. 10. Time to impregnate (= impregnation time) (a) microporous and (b) macroporous samples as a function of sintering temperature and Ca/P ratio according to the full-dip method. For each temperature, three results are presented, corresponding to a composition of (from left to right): Ca/P = 1.45 (hatched bars); Ca/P = 1.475 (white bars); Ca/P = 1.50 (gray/dotted bars).

lary pressure; (ii) the liquid rises on both sides of a U-shaped capillary, and capillary rise stops when the pressure of the trapped air has reached the capillary pressure of both sides of the U-shaped pore, (iii) the capillary pressure is counterbalanced by the force of gravity (for vertical pores) [29,30]; and (iv) the capillary pressure is lower than the pressure p_b required to create an air bubble (when the air has to exit the capillary through a liquid). This pressure is expressed by Laplace equation:

$$p_b = \frac{2\gamma}{r_b} \tag{2}$$

In this equation, γ is the surface energy of the water–air interface, and r_b is the radius of the extremity contacting water. Comparing Eqs. (1) and (2), it appears that a capillary rise into a scaffold dipped in a liquid cannot occur if the following condition is not met:

$$r_c \leq r_b \cos \theta \tag{3}$$

So, if the scaffold pores are all of the same size ($r_c = r_b$), the only possibility for air to leave the porous scaffold is when the solid surface is perfectly wetted by the liquid ($\cos \theta = 1$), which is unlikely to happen. This observation underlines the need to have a porous network made of pores of various sizes to enable an extensive degree of impregnation, the small pores acting as “water pumps” and the large ones acting as “exhaust pipes”.

In the present study, not only the extent, but also the rate of impregnation was determined. The relation between the impregnation rate and the capillary geometry can be extracted from the combination of Eq. (1) and the Hagen–Poiseuille law, which relates the flow rate Q of a Newtonian liquid through a cylindrical channel (here a capillary), to its viscosity μ , the capillary dimensions (radius r_c , length L_c) and the difference in pressure ΔP :

$$Q = \frac{\pi r^4}{8 \mu L} \cdot \Delta P \tag{4}$$

Assuming that $\Delta P = P_c$, Eqs. (1) and (4) can be combined to obtain the mean liquid velocity in the capillary, v :

$$v = \frac{\gamma \cos \theta}{4 \mu L} \cdot r \tag{5}$$

This equation also called the Washburn equation [31] indicates that the flow rate within a capillary (expressed by the mean liquid velocity in m s^{-1}) is proportional to the capillary radius. A similar relation would be found by including gravity forces because gravity forces are not affected by the pore radius [29].

Using these theoretical considerations, it is easier to understand the experimental results generated in the present study. Therefore, the aim of the next paragraphs is to review the various experimental results and propose an interpretation.

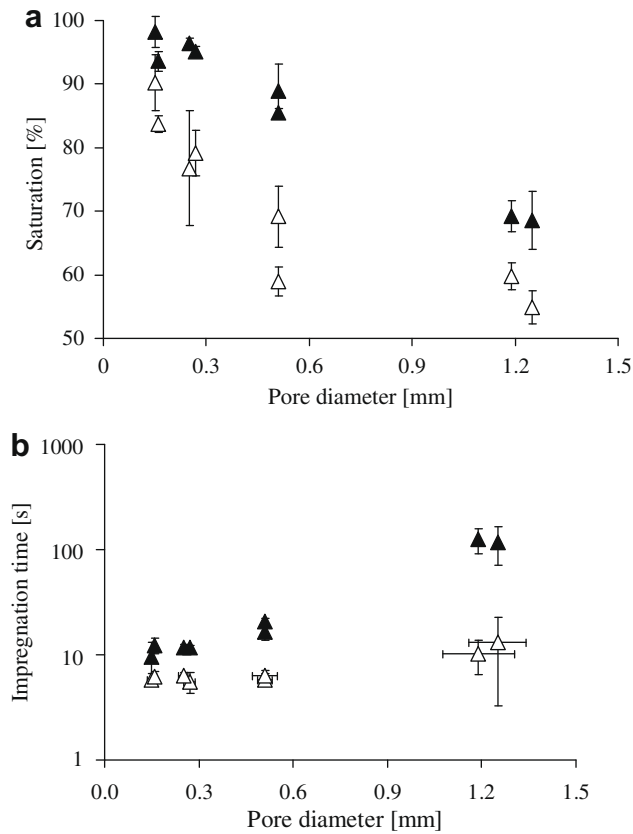


Fig. 11. (a) Saturation levels and (b) impregnation time results in (▲) partial-dip and (△) full-dip experiments of porous blocks with constant porosity ($52 \pm 2\%$) [12], but various macropore diameters.

The first interesting observation is that microporous samples were not fully filled with liquid (Figs. 7 and 8), suggesting that a certain number of micropores were either closed or U-shaped. Looking at the SEM photos (Figs. 3 and 4), the second explanation appears to be the most likely. It is worth mentioning here that similar saturation results (partial saturation) were observed by Williams when testing filter paper [32]. A second interesting observation is that the degree of impregnation of all the blocks tested was lower in the fully dipped state compared with the partially dipped state (Figs. 7 and 8). This difference suggests that in the fully dipped state the need to create an air bubble in water prevents to some extent the release of air from the scaffolds (Laplace equation, Eq. (2)). Another result of interest is that the presence of macropores had a detrimental effect on the degree of impregnation of emulsified samples (compare Figs. 7a and 8a with Figs. 7b and 8b), despite the fact that these pores were fully open due to the presence of an open microporosity (Figs. 3 and 4). This effect was particularly strong for large macropores (Fig. 11a). Here, it is speculated that micropores were invaded by water at a faster rate than macropores were, hence trapping air in macropores solely surrounded by micropores. According to the Washburn equation, small pores should be invaded by water at a slower pace than large pores. However, as underlined by Bico et al. [33], the assumption that a porous interconnected network can be simulated with a set of single capillaries is an over-simplification of reality. These authors proposed to model such a network with an array of capillary tubes decorated with a texture on their walls, and predicted that the capillary rise in such a network occurs much faster in smaller pores than in larger pores, larger pores acting as water reservoir for smaller pores. The entrapment of air in macropores might explain why macroporous samples had lower saturation levels than microporous samples did. The sharp decrease in saturation level with an increase in

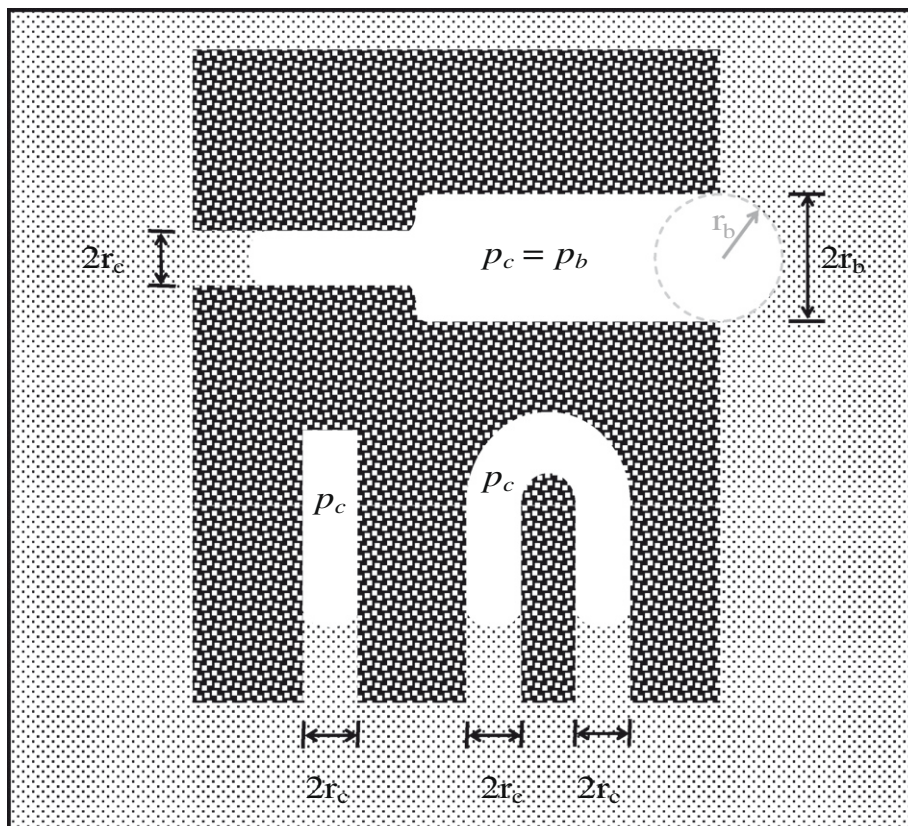


Fig. 12. Schematic representation of capillary rise into a closed pore, into a U-shaped pore and into an open pore.

macropore size (Fig. 11a) suggests that the effect proposed by Bico et al. [33] strongly depends on the difference between the size of small and large pores: the bigger the difference, the lower the saturation level. Interestingly, the saturation level of samples sintered at various temperatures increased at higher sintering temperatures, i.e., when the micropore size increased or when the difference between micropore and macropore size decreased. This effect was particularly strong for a Ca/P molar ratio of 1.45, for which the strongest change in micropore size was observed (Figs. 3 and 4).

In the previous paragraph, it was shown that several experimental results could be easily related to theoretical considerations. Other experimental results are more difficult to explain. For example, the impregnation rate was hardly affected by a change in micropore size (see change due to sintering temperature; Figs. 3, 4, 9 and 10), even though Eq. (9) predicts that an increase in capillary radius (or pore size) should increase the rate of capillary rise. Furthermore, the comparison of saturation (Figs. 7 and 8) and impregnation time (Figs. 9 and 10) shows that high saturation levels are associated with short impregnation times. This result is surprising, since more liquid has to be absorbed when the saturation level is high. But apparently, the high driving force that leads to a high saturation level is also large enough to increase the impregnation rate.

To summarize, the present study shows that it is not easy to fully impregnate porous scaffolds with a liquid, particularly when the scaffolds simultaneously contain micropores and large macropores. Saturation levels of 60–70% are not exceptional, even though the scaffolds are fully interconnected. The use of vacuum cycles can increase the saturation level but, for some porous scaffolds, even vacuum cycles at 0.1 atm do not lead to full impregnation (data not shown here). This study is probably the first study on the topic, and only a few parameters have been looked at, but the results presented here clearly underline the need to study this problem in more detail. It is generally assumed that scaffolds placed in a cell culture are fully invaded by the cell-culture medium and that cells can penetrate the scaffolds, provided the pore interconnections are large enough for cell penetration. The present results suggest that cells might not be able to fully invade a porous scaffold owing to the presence of air bubbles.

5. Conclusion

Microporous and macroporous scaffolds with various micropore and macropore sizes were impregnated in water according to two modes: the partial-dip mode, in which the blocks were only partially dipped in water, and the full-dip mode, in which the blocks were fully dipped in water. Even though all samples had an open porosity, not all samples could be fully impregnated, particularly in the full-dip mode. Specifically, saturation levels ranged between 50% and 100%, most of them being close to 70–80%. The saturation level was strongly affected by the macropore size: the bigger the pores, the lower the saturation levels. The time to full impregnation was in the order of a few dozen seconds and decreased with an increase in saturation. This study underlines the need to investigate scaffold impregnation further, particularly when the scaffolds are meant to be used in cell culture media. The presence of air might prevent cell proliferation.

Appendix A

This appendix describes how the sample porosity and the saturation level in the partial-dip and full-dip modes were calculated. First, the porosity of the blocks P was determined using the following equation:

$$P = \left(1 - \frac{\rho_{block}}{\rho_{\beta TCP}} \right) \quad (6)$$

where ρ_{block} is the apparent block density and $\rho_{\beta TCP}$ is the β -TCP theoretical density ($= 3.14 \text{ g cm}^{-3}$). ρ_{block} is given by:

$$\rho_{block} = \frac{W_{dry}}{V_{Cyl}} \quad (7)$$

where V_{Cyl} is the cylinder volume ($= 2.16 \text{ cm}^3$). The saturation S (defined as the percentage of the porosity that is filled with water) was then determined using different formulas according to the different dipping methods:

$$S = \frac{V_{Water}}{V_{Porosity}} = \frac{W_{abs}}{P \cdot V_{Cyl} \cdot \rho_{H_2O}} \quad (\text{partial dip}) \quad (8)$$

$$S = \frac{V_{Water}}{V_{Porosity}} = \frac{\Delta W + V_{Cyl} \cdot \rho_{H_2O} + 0.05g}{P \cdot V_{Cyl} \cdot \rho_{H_2O}} \quad (\text{full dip}) \quad (9)$$

In these equations, ρ_{H_2O} is the density of water. The term $V_{Cyl} \cdot \rho_{H_2O}$ in Eq. (9) compensates for the Archimedes force of the block, and the term 0.05 g corrects the Archimedes force of the part of the thin metallic brace dipped in water. The impregnation time was also measured for each sample. It was defined as the time between the start of dipping and the attainment of a weight remaining constant ($\pm 0.01 \text{ g}$) for at least 30 s. The precision was, however, limited to $\pm 4 \text{ s}$ (time increment for data collection). For each composition and/or sintering temperature, three different samples (only one or two in the case of samples without macro porosity) were tested, and the mean value of the saturation was calculated. All the tests were repeated three times, thus providing nine values per condition.

Considering the fact that macroporous blocks contained micropores and macropores, it is of interest to determine the fraction of microporosity and macroporosity. Several methods can be used which all give similar values (see also Fig. 5). One method of determining macroporosity is based on the sample composition and the shrinkage during sintering. This method assumes that the setting reaction occurs at a constant volume and that macroporosity produced by paraffin remains constant during sintering. Past studies have shown good agreement between these values and those determined by μCT [11,12]. The microporosity is then defined as the difference between the total porosity and the macroporosity. Another method is μCT , since μCT only detects macropores. The third method that can be used is to infer the microporosity of macroporous samples based on the total porosity of microporous samples. For that purpose, it must be assumed that the microstructure is not influenced by the presence of macropores, which was unfortunately only partly supported by the SEM images (Fig. 3). The block porosity of macroporous blocks, $P_{b,ma}$, is given by:

$$P_{b,ma} = \frac{V_{microp,ma} + V_{macrop,ma}}{V_{tot,ma}} \quad (10)$$

where $V_{tot,ma}$ is the total cylinder volume, and $V_{microp,ma}$ and $V_{macrop,ma}$ are the volumes of the microporosity and macroporosity of macroporous samples. The above hypothesis now allows the block porosity of microporous blocks, $P_{b,mi}$, as determined in the tests, to be equated with the microporosity of the macroporous blocks:

$$P_{b,mi} = \frac{V_{microp,mi}}{V_{tot,mi}} = \frac{V_{microp,ma}}{V_{tot,ma} - V_{macrop,ma}} \quad (11)$$

where $V_{microp,mi}$ is the total porous volume of the microporous samples. Inserting Eq. (11) into Eq. (10), one obtains:

$$P_{b,ma} = \frac{P_{b,mi}(V_{tot,ma} - V_{macrop,ma}) + V_{macrop,ma}}{V_{tot,ma}} \quad (12)$$

and rearranging Eq. (12) one can determine the macroporosity P_{ma} of the macroporous blocks:

$$P_{ma} = \frac{V_{macrop,ma}}{V_{tot,ma}} = \frac{P_{b,ma} - P_{b,mi}}{1 - P_{b,mi}} \quad (13)$$

The microporosity P_{mi} is given simply by the difference between the total block porosity and the macroporosity:

$$P_{mi} = \frac{V_{microp,ma}}{V_{tot,ma}} = P_{b,ma} - P_{ma} \quad (14)$$

For P_{ma} and P_{mi} , the inherited errors which increased as a result of the calculations were taken into account. They were defined as the absolute difference between the maximally aberrant result, calculated with the mean values of $P_{b,mi}$ and $P_{b,ma}$ plus or minus their standard deviations, and the result calculated simply with the mean values.

Appendix B. Figures with essential colour discrimination

Certain figures in this article, particularly Figure 1, are difficult to interpret in black and white. The full colour images can be found in the on-line version, at doi:10.1016/j.actbio.2010.01.018.

References

- [1] Cutright DE, Bhaskar SN, Brady JM, Getter L, Posey WR. Reaction of bone to tricalcium phosphate ceramic pellets. *Oral Surg Oral Med Oral Pathol* 1972;33:850–6.
- [2] Levitt SR, Crayton PH, Monroe EA, Condrate RA. Forming method for apatite prostheses. *J Biomed Mater Res* 1969;3:683–4.
- [3] Monroe EA, Votava W, Bass DB, McMullen J. New calcium phosphate ceramic material for bone and tooth implants. *J Dent Res* 1971;50:860–1.
- [4] Gaasbeek RD, Toonen HG, van Heerwaarden RJ, Buma P. Mechanism of bone incorporation of beta-TCP bone substitute in open wedge tibial osteotomy in patients. *Biomaterials* 2005;26:6713–9.
- [5] van Hemert WL, Willems K, Anderson PG, van Heerwaarden RJ, Wymenga AB. Tricalcium phosphate granules or rigid wedge preforms in open wedge high tibial osteotomy: a radiological study with a new evaluation system. *Knee* 2004;11:451–6.
- [6] Levin MP, Getter L, Cutright DE. A comparison of iliac marrow and biodegradable ceramic in periodontal defects. *J Biomed Mater Res* 1975;9:183–95.
- [7] Karageorgiou V, Kaplan D. Porosity of 3D biomaterial scaffolds and osteogenesis. *Biomaterials* 2005;26:5474–91.
- [8] Lu JX, Flautre B, Anselme K, Hardouin P, Gallur A, Descamps M, et al. Role of interconnections in porous bioceramics on bone recolonization in vitro and in vivo. *J Mater Sci Mater Med* 1999;10:111–20.
- [9] von Doernberg MC, von Rechenberg B, Bohner M, Grünenfelder S, van Lenthe GH, Muller R, et al. *In vivo* behavior of calcium phosphate scaffolds with four different pore sizes. *Biomaterials* 2006;27:5186–98.
- [10] Bohner M. Calcium phosphate emulsions: possible applications. *Key Eng Mater* 2001;192–195:765–8.
- [11] Bohner M, van Lenthe GH, Grünenfelder S, Hirsiger W, Evison R, Muller R. Synthesis and characterization of porous beta-tricalcium phosphate blocks. *Biomaterials* 2005;26:6099–105.
- [12] Bashoor-Zadeh M, Baroud G, Bohner M. Geometric analysis of porous bone substitutes using micro-computed tomography and fuzzy distance transform. *Acta Biomater* 2010;6:864–75.
- [13] van Lenthe GH, Hagenmuller H, Bohner M, Hollister SJ, Meinel L, Muller R. Nondestructive micro-computed tomography for biological imaging and quantification of scaffold-bone interaction in vivo. *Biomaterials* 2007;28:2479–90.
- [14] Rodriguez-Carvajal J. Recent developments of the program FULLPROF. *Commission Powder Diffr (IUCr) Newsl* 2001;26:12–9.
- [15] Dickens B, Schroeder LW, Brown WE. Crystallographic studies on the role of Mg as a stabilizing impurity in β -Ca₃(PO₄)₂. *J Solid State Chem* 1974;10:232–48.
- [16] Mathew M, Schroeder LW, Dickens B, Brown WE. The crystal structure of α -Ca₃(PO₄)₂. *Acta Cryst* 1977;B33:1325–33.
- [17] Sudarsanan K, Young RA. Significant precision in crystal structure details: holly springs hydroxyapatite. *Acta Cryst* 1969;B25:1534–43.
- [18] Boudin S, Grandin A, Borel MM, Leclaire A, Raveau B. Redetermination of the β -Ca₂P₂O₇ structure. *Acta Cryst C* 1993;49:2062–4.
- [19] Bohner M, Doebelin N, Baroud G. Theoretical and experimental approach to test the cohesion of calcium phosphate pastes. *Eur Cell Mater* 2006;12:26–35.
- [20] Descamps M, Hornez JC, Leriche A. Effects of powder stoichiometry on the sintering of β -tricalcium phosphate. *J Eur Ceram Soc* 2007;27:2401–6.
- [21] Famery R, Richard N, Boch P. Preparation of alpha-tricalcium and beta-tricalcium phosphate ceramics, with and without magnesium addition. *Ceram Int* 1994;20:327–36.
- [22] Itatani K, Nishioka T, Seike S, Howell FS, Kishioka A, Kinoshita M. Sinterability of β -calcium orthophosphate powder prepared by spray-pyrolysis. *J Am Ceram Soc* 1994;77:801–5.
- [23] Miranda P, Saiz E, Gryn K, Tomsia AP. Sintering and robocasting of β -tricalcium phosphate scaffolds for orthopaedic applications. *Acta Biomater* 2006;2:457–66.
- [24] Ryu HS, Youn HJ, Hong KS, Chang BS, Lee CK, Chung SS. An improvement in sintering property of beta-tricalcium phosphate by addition of calcium pyrophosphate. *Biomaterials* 2002;23:909–14.
- [25] Akao M, Aoki H, Kato K, Sato A. Dense polycrystalline β -tricalcium phosphate for prosthetic applications. *J Mater Sci* 1982;17:343–6.
- [26] Raynaud S, Champion E, Lafon JP, Bernache-Assollant D. Calcium phosphate apatites with variable Ca/P atomic ratio III. Mechanical properties and degradation in solution of hot pressed ceramics. *Biomaterials* 2002;23:1081–9.
- [27] Carrodegus RG, De Aza AH, Turrillas X, Pena P, De Aza S. New approach to the beta-alpha polymorphic transformation in magnesium-substituted tricalcium phosphate and its practical implications. *J Am Ceram Soc* 2008;91:1281–6.
- [28] Fisher LR, Lark PD. An experimental study of the washburn equation for liquid flow in very fine capillaries. *J Colloid Interface Sci* 1979;69:486–92.
- [29] Marmur A, Cohen RD. Characterization of porous media by the kinetics of liquid penetration: the vertical capillaries model. *J Colloid Interface Sci* 1997;189:299–304.
- [30] Zhmud BV, Tiberg F, Hallstenson K. Dynamics of capillary rise. *J Colloid Interface Sci* 2000;228:263–9.
- [31] Washburn EW. The dynamics of capillary flow. *Phys Rev* 1921;17:273–83.
- [32] Williams R. The capillary without walls. *J Colloid Interface Sci* 1981;79:287–8.
- [33] Bico J, Thiele U, Quéré D. Wetting of textured surfaces. *Colloids Surf A Physicochem Eng Aspects* 2002;206:41–6.